Analytica Chimica Acta xxx (xxxx) xxx

Contents lists available at ScienceDirect

Analytica Chimica Acta

journal homepage: www.elsevier.com/locate/aca

ZnCuInSe/Au/TiO_2 sandwich nanowires-based photoelectrochemical biosensor for ultrasensitive detection of kanamycin

Hongchao Geng [a], Xiaoxu Chen [b], Leilei Sun [a], Yan Qiao [a], Jie Song [a], Sisi Shi [a], Qingyun Cai [a, *]

[a] State Key Laboratory of Chemo/Biosensing and Chemometrics, College of Chemistry and Chemical Engineering, Hunan University, Changsha, 410082, PR China

[b] Shenma Tire Cord Development Co. Ltd, Pingdingshan, 467000, PR China

HIGHLIGHTS

- ZnCuInSe quantum dots was used for the first time to constructed the ZnCuInSe/Au/TiO_2 sandwich nanowires photoelectrode.
- Au NPs serve as photosensitizer and electron relay facilitating light to electron conversion and charge transfer.
- The PEC sensor for the detection of kanamycin was developed using ZnCuInSe/Au/TiO_2 as substrate with a LOD down to 0.2 nM.
- ZnCuInSe/Au/TiO_2 nanowires can detectionof different biomolecules by modifying various recognizers.

GRAPHICAL ABSTRACT

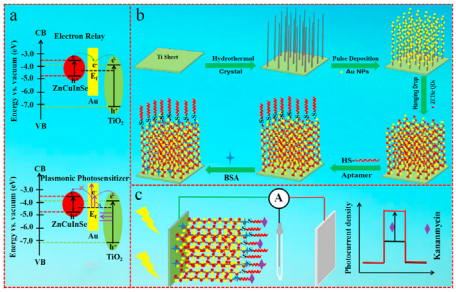

ARTICLE INFO

Article history:
Received 24 August 2020
Received in revised form
10 November 2020
Accepted 13 November 2020
Available online xxx

Keywords:
Photoelectrochemical
TiO_2 nanowires
ZnCuInSe QDs
Kanamycin

ABSTRACT

A highly selective and sensitive photoelectrochemical (PEC) sensing platform was developed for kanamycin assay based on the aptamer modified sandwich-structured ZnCuInSe/Au/TiO_2 nanowires. Sandwiched between the TiO_2 nanowires and the ZnCuInSe quantum dot (QDs) layer, the Au nanoparticles (Au NPs) serves as a plasmonic photosensitizer and an electron relay, which expand the light absorption range and facilitates the charge transfer. Also, ZnCuInSe QDs, a broad spectrum photosensitizer can capture visible light, which enhance the photocurrent density response. Through the Au−S bond and Cu−S bond, the HS-aptamer were immobilized on the ZnCuInSe/Au/TiO_2 nanowires as a recognition unit for kanamycin. The proposed sensing platform showed excellent assay performance for kanamycin with a linear response range from 0.2 to 250 nM, and high selectivity. By changing the recognizers, the proposed sensing platform could be easily extended to detect other biomolecules, and may have a promising application in bioanalysis.

1. Introduction

In recent years, PEC bioassay has aroused great attention because it combines the advantages of optics methods and electrochemical sensors [1–3]. Moreover, it possess attractive

* Corresponding author.
E-mail address: qycai0001@hnu.edu.cn (Q. Cai).

https://doi.org/10.1016/j.aca.2020.11.017
0003-2670/

advantages such as a simple device, easy operation, low background signal, and good sensitivity and low cost [4,5]. Also, high selectivity can be achieved by applying antibodies [6], aptamers [7] and enzymes [8] as biological recognition element. Compared with antibodies and enzymes, aptamers have inherent binding affinity that can bind to their targets with high specificity [9] and they are less sensitive to temperature and pH, therefore less prone to deactivation [10].

On the other hand, semiconductors were often used as light trapping materials to construct PEC sensors and Titanium dioxide (TiO_2) has been widely applied due to its good photocatalytic activity, stability, and controllable morphology [11,12]. Vertically aligned TiO_2 nanowires have much high surface area and excellent electron transport paths, which can increase the light absorption [13]. However, it can only absorb ultraviolet light because of its wide band gap (3.2 eV), the ultraviolet light can cause some damage to the biological molecules on the sensors, thus limiting the biological applications of the sensor [14]. Also, the fast recombination of photogenerated electron−hole pairs may recede the PEC signal [15]. The combination of TiO_2 and noble metals (Au, Ag) and/or narrow band gap semiconductors, such as CdS, CdSe and PbS QDs, can expanded the absorption range to visible light and inhibited the recombination of electron hole pairs. For example, Wang's group utilized graphene modified TiO_2 nanotube arrays to develop a PEC chloramphenicol sensor, which exhibited a low detection limit of 57.9 pM [16]. Ghorbani adopted the Au NPs decorated TiO_2 nanorods photoelectrode to detection of Cr(VI) with a very low detection limit of 0.006 μM [17].

More recently, Pb, Cd-free Zn doped $CuInSe_2$ (ZnCuInSe) QDs have attracted considerable attention owing to its less-toxicity, narrow bandgap (1.05 eV) and superior optical properties. In addition, doped QDs not only ameliorate the stability and lessen the defects due to the firm lattice structure and lessened atomic intradiffusion, but also favor the electron transfer due to the move up of conduction band edge [18−20]. Therefore, doped QDs can be used as an excellent light-harvesting sensitizers. As an example, Du et al. constructed QDs sensitized solar cells with Cd-, Pb-free ZnCuInSe QDs as effective light harvesters, the cells were demonstrated to significantly improve the power conversion efficiency due to the ZnCuInSe QDs [21]. Analogously, as an highly narrow bandgap semiconductor, ZnCuInSe QDs could match well with the TiO_2 nanowires with a cascade energy level positioning to accomplish high light absorption and conversion efficiency. To the best of our knowledge, a ternary nanocomposite based Au NPs and ZnCuInSe QDs has not yet been constructed and utilized within a PEC platform.

Therefore, in this work, a visible-light driven PEC aptasensor based on aptamer-modified ZnCuInSe/Au/TiO_2 nanocomposites was present for the analysis of kanamycin that is widely applied as a broad-spectrum antibiotic because of its low cost and effective treat infections caused by most of bacteria [22]. However, the overuse in animal-derived foods can lead to hazards to human health, including anaphylactic shock, diarrhea, vomiting, hearing loss and kidney damage [23,24]. Therefore, it is necessary to establish a highly sensitive and selective strategy for the detection of kanamycin. In our work, the Au NPs sandwiched between the TiO_2 nanowires and the ZnCuInSe QDs layer play a dual role in enhancing the photocurrent, as shown in Scheme 1a. On the one hand, it acts as a photosensitizer, which extends the photoabsorption of the electrode to visible range. On the other hand, it serves as an electron relay, which facilitates charge transfer between the ZnCuInSe QDs and TiO_2 nanowires. The presence of ZnCuInSe QDs can expand the absorption to visible light region of the composite, thus enduing the matrix with a superior light absorption capacity. Also, the aptamers of kanamycin were immobilized on ZnCuInSe/Au/TiO_2 photoelectrode via Au−S and Cu−S to form an aptasensor [25]. In the presence of kanamycin, the aptamer on the ZnCuInSe/Au/TiO_2 photoelectrode could specifically and sensitively capture kanamycin that are oxidized by the photogenerated holes. The recombination rate of photogenerated electron-hole pairs are inhibited, which lead to a amplified in photocurrent density response, as illustrated in Scheme 1c.

2. Experimental section

2.1. Materials and apparatus

The materials and apparatus are described in the Supplementary Material.

2.2. Preparation of TiO_2 nanowires and ZnCuInSe QDs

The detailed experimental steps are described in the Supplementary Material.

2.3. Fabrication of ZnCuInSe/Au/TiO_2 nanowires sandwich structure

ZnCuInSe/Au/TiO_2 composite electrode was prepared according to a multistep procedure illustrated in Scheme 1b. The Au/TiO_2 electrode was constructed firstly by pulse-electrical deposition using $HAuCl_4$ (1 mM) as the electrolyte. The procedure was carried out in a three-electrode system with an Ag/AgCl reference electrode, platinum counter electrode, and the TiO_2 nanowires as working electrode [26]. The electrodeposition process was conducted at deposition potential −6.0 V for 0.2 s, and then -10^{-5} V for 1 s, using a certain sequential pulses to obtain the optimal load of Au NPs. Subsequently, the Au/TiO_2 nanowires was washed with DI water and dried at 60 °C for further use.

ZnCuInSe/Au/TiO_2 nanowires was fabricated by dropping 10 μL of the as-prepared ZnCuInSe QDs aqueous solution (7 mg/mL) on the Au/TiO_2 nanowires, then dried at 50 °C, which were repeated until that the optimal load of ZnCuInSe QDs was achieved.

2.4. Fabrication of PEC aptasensor

The aptamer was immobilized onto ZnCuInSe/Au/TiO_2 electrode via Au−S and Cu−S bond between Au NPs, ZnCuInSe QDs and the aptamer. 30 μL of aptamer solution was dropped onto the ZnCuInSe/Au/TiO_2 electrode and incubated for 24 h, and rinsed with washing solution to remove unbound aptamers. In order to reduce the nonspecific adsorption, 30 μL of 1% BSA blocking buffer solution was dropped on the electrode to block nonspecific binding sites. After 2 h, the electrodes were rinsed and dried for further use.

2.5. Electrochemical measurements

The photocurrent density were measured in a standard three-electrode system with the as-prepared materials as working electrode, a Pt counter electrode, and a Ag/AgCl reference electrode. The PEC activity of different electrode were determined in an electrolyte containing 0.35 M Na_2SO_3 and 0.24 M Na_2S. Immunoassay was measured in an aqueous solution of PBS (pH = 7.4) that contains 0.08 M of ascorbic acid (AA): AA was utilized as an electron donor to capture holes and enhanced the photocurrent density. A 500 W Xe lamp was regarded as the light source at a light density of 100 mW/cm^2.

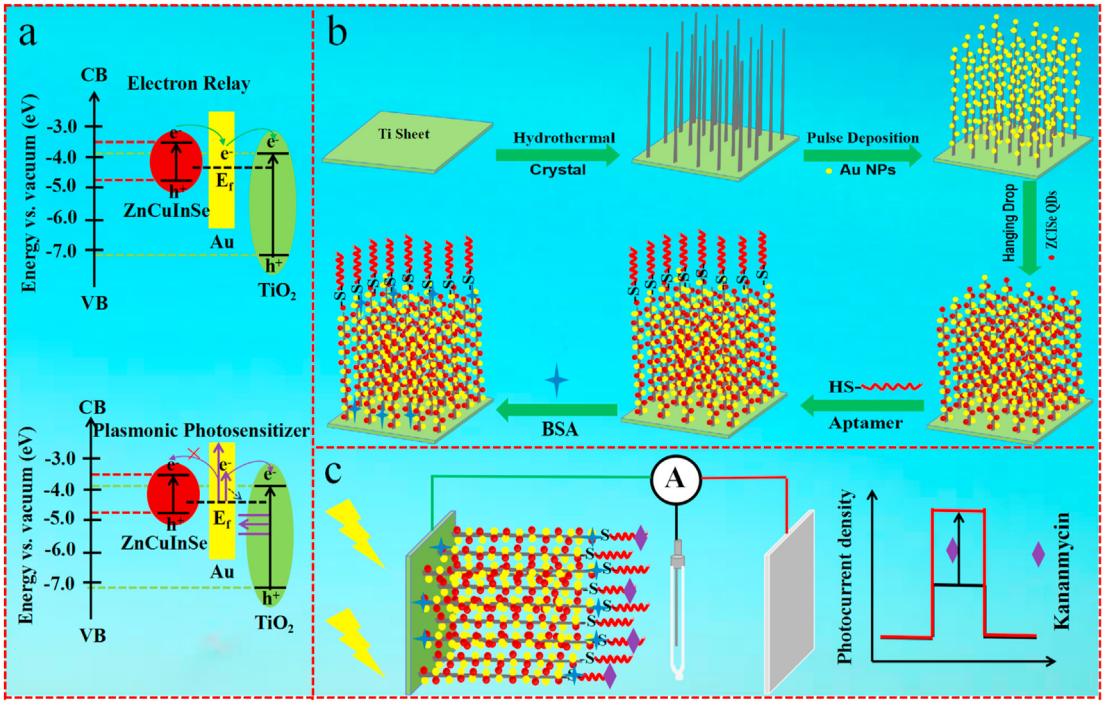

Scheme 1. (a) Dual role of Au NPs in the ZnCuInSe/Au/TiO_2 sandwich structure. Construct of ZnCuInSe/Au/TiO_2 nanowires photoelectrode; fabrication steps of the aptasensor (b) and its PEC mechanism for detection (c). CB = conduction band, VB = valence band, E_f = Fermi energy level.

3. Results and discussion

3.1. Characterization of the synthesized materials

The SEM images of Fig. 1A reveals the morphology of pure TiO_2 nanowires at low and high magnifications, respectively. Vimineous TiO_2 nanowires had an average diameter of 40 nm and their surface was smooth. In Fig. 1B, the SEM of Au/TiO_2 nanowires composite revealed that Au NPs were deposited on the TiO_2 nanowires by pulse-electrical deposition. Also, Fig. S1 displays the SEM images of Au/TiO_2 with different cycles of pulse deposition. With increase of the number of deposition cycles, the amount of Au NPs changed from less to more, and then the size become large and agglomeration. Fig. 1C shows the TEM image of ZnCuInSe/Au/TiO_2 nanowires, a large number of gray particles of about 8 nm were observed on the surface of nanowires, demonstrating the successful deposition of ZnCuInSe QDs on the Au/TiO_2 nanowires. Moreover, the composite electrode was confirmed by the HRTEM, as shown in Fig. 1D, the lattice fringe with spacing of 0.35 nm, 0.24 nm and 0.32 nm correspond to the (101) plane of anatase TiO_2, (111) plane of Au NPs and the (111) plane of ZnCuInSe QDs, indicating that the as-prepared electrode consists of TiO_2, Au and ZnCuInSe QDs. Additionally, the EDS results show that the elements of Ti, O, Au, Zn, Cu, In and Se exist in the ZnCuInSe/Au/TiO_2 nanowires. XRD analysis was used to further investigate the crystalline structure and phase composition of the ZnCuInSe/Au/TiO_2 nanocomposite, as shown in Fig. 1F. Compared with the pure Ti sheet, the XRD pattern of TiO_2 nanowires shows the distinct characteristic diffraction peaks at $2\theta = 25.29°$ and 48°, corresponding to the crystal planes of (101) and (200) of the anatase TiO_2, respectively. In addition to the characteristic peaks of Ti and TiO_2 nanowi, the XRD spectra of Au/TiO_2 electrode displayed the peaks at $2\theta = 44.3°$ and 64.54°, which can be assigned to (200) and (220) crystallographic planes of Au NPs, respectively. When compared with Au/TiO_2, ZnCuInSe/Au/TiO_2 nanowires exhibited two new peaks at 27° and 43.4°, corresponding to the crystal planes of (111) and (220) of the ZnCuInSe QDs, which is in good agreement with the HRTEM results. It should be noted that the intensity of the diffraction peaks at $2\theta = 25.29°$ gradually decreases with the loaded of Au and ZnCuInSe, suggesting that the successful deposition of Au NPs and ZnCuInSe QDs. Weak diffraction peak of Au and ZnCuInSe was observed as the concentration was low.

Fig. 2A shows the UV–vis absorption spectra of TiO_2 and ZnCuInSe/TiO_2 nanowires in the absence and presence of Au NPs. TiO_2 nanowires displayed a sharp absorption edge at around 395 nm. After the immobilization of the ZnCuInSe QDs onto TiO_2 nanowires, the absorption edge red shift to 425 nm. The presence of Au NPs embedded between TiO_2 and ZnCuInSe QDs further increased the absorption range up to 695 nm. The strong absorption band centered at 545 nm and 566 nm corresponded to the localized surface plasmon resonance (LSPR) of the Au NPs [27] and the absorption of ZnCuInSe QDs, respectively. The LSPR peak of the Au NPs sandwiched between the TiO_2 nanowires and the ZnCuInSe QDs layer red shift due to the large refractive index of the ZnCuInSe QDs. In addition, the band gaps of electrode were calculated using Tauc relation (eqn (1)) [28] according to the UV–vis absorption spectra, as shown in Fig. 2B. The band gap of TiO_2, ZnCuInSe/TiO_2, Au/TiO_2 and ZnCuInSe/Au/TiO_2 nanowires were 3.25, 3.1, 2.9, and 2.75 eV, respectively.

$$\alpha h\nu = \sqrt{A\ (h\nu - Eg)} \quad (1)$$

Where Eg is the bandgap energy, hν refers to the photon energy and α represents absorption coefficient.

Photoluminescence spectra have been widely used to study the electron/hole lifetime. A higher fluorescence intensity means a higher recombination rate of photogenerated electrons/holes, and hence a shorter lifetime of photogenerated carriers [29,30]. Fig. 2C proves the photoluminescence spectrum of TiO_2, Au/TiO_2, ZnCuInSe/TiO_2 and ZnCuInSe/Au/TiO_2 nanowires. The order of

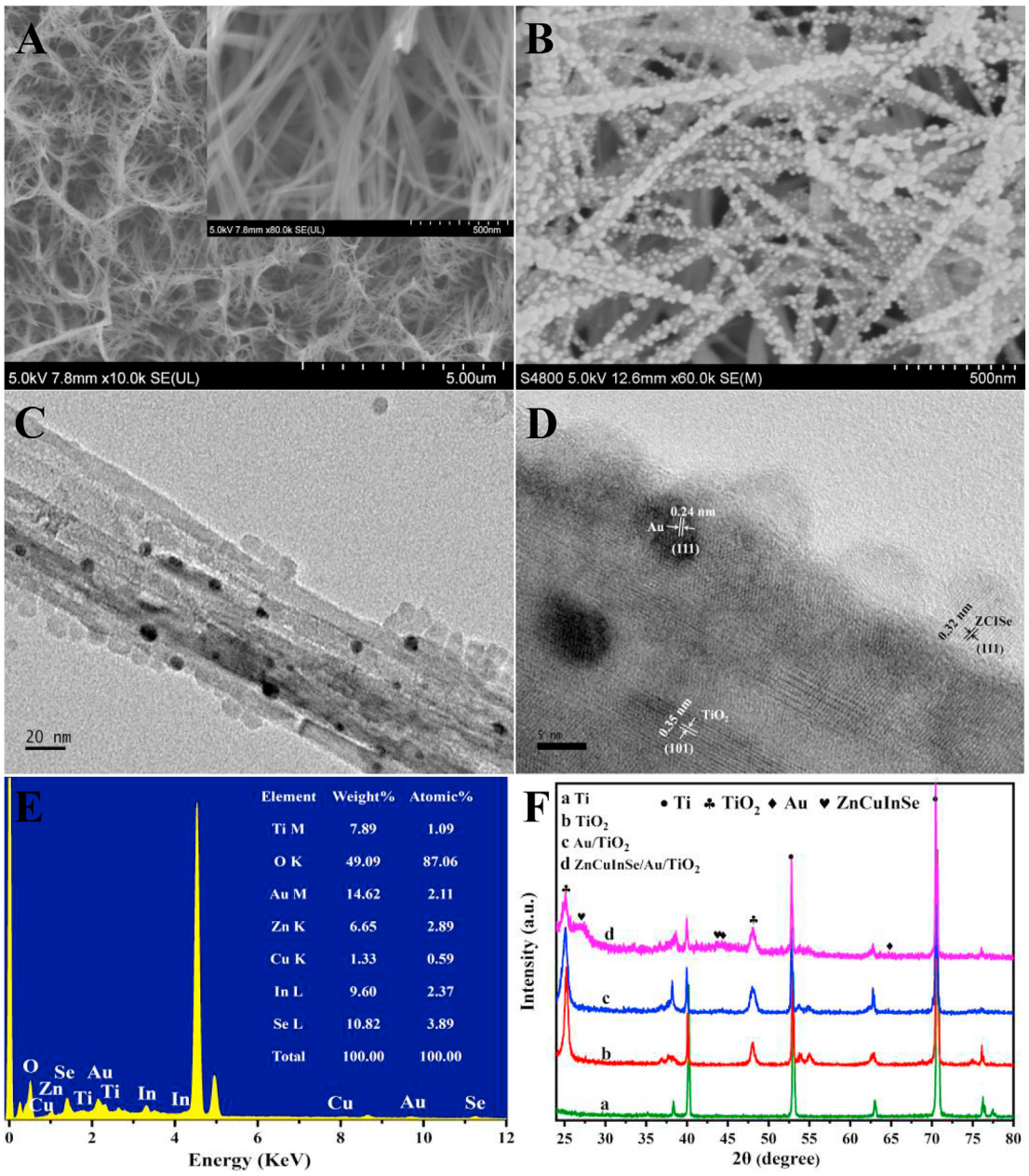

Fig. 1. SEM images of TiO_2 nanowires with low (A) and high (Inset of A) magnification, SEM images of Au/TiO_2 (B), TEM images (C), HRTEM (D), EDS images (E) and XRD patterns of $ZnCuInSe/Au/TiO_2$ naowires.

photoluminescence intensity is Au/TiO_2 < $ZnCuInSe/TiO_2$ < TiO_2, which represents the modification Au NPs or ZnCuInSe QDs decreases the recombination rate of photogenerated electrons/holes. The photoluminescence intensity of Au/TiO_2 was weaker than $ZnCuInSe/Au/TiO_2$ is due to the loading of the ZnCuInSe QDs which increase the light capture efficiency and generating more photogenerated carriers. More photogenerated carriers suggest a higher probability for recombination of photogenerated electron-hole pairs.

Also, the loading amount of the sensitizers was opimized to obtain a high sensitivity. As shown in Fig. S2A, the photocurrent density of Au/TiO_2 nanowires increased with the rise of the deposition sequences until 70, above which the photocurrent density quickly dropped for the agglomeration of the Au NPs, big Au blocks would have less electron transfer efficiency [31]. From Fig. S2B, the maximum photocurrent density of $ZnCuInSe/Au/TiO_2$ nanowires was obtained when 30 μL of ZnCuInSe QDs was loaded. It was about 10 and 3.4 times that obtained on TiO_2 nanowires and Au/TiO_2 nanowires, respectively. In addition, the photocurrent density is higher than $CuInSe_2/Au/TiO_2$ nanowires with same volume of quantum dot solution, as shown in Fig. S2C, indicating the excellent optical properties of Zn doped $CuInSe_2$ QDs. However, excess ZnCuInSe QDs caused more resistance, which could hinder the electron transferred to TiO_2 nanowires. In the following experiments, the $ZnCuInSe/Au/TiO_2$ nanowires was fabricated with the optimal composition.

Fig. 2D shows the photocurrent density responses of TiO_2, Au/TiO_2, $ZnCuInSe/TiO_2$ and $ZnCuInSe/Au/TiO_2$ nanowires at applied potential of 0 V under visible-light irradiation. The photocurrent density of $ZnCuInSe/Au/TiO_2$ nanowires was greater than the sum

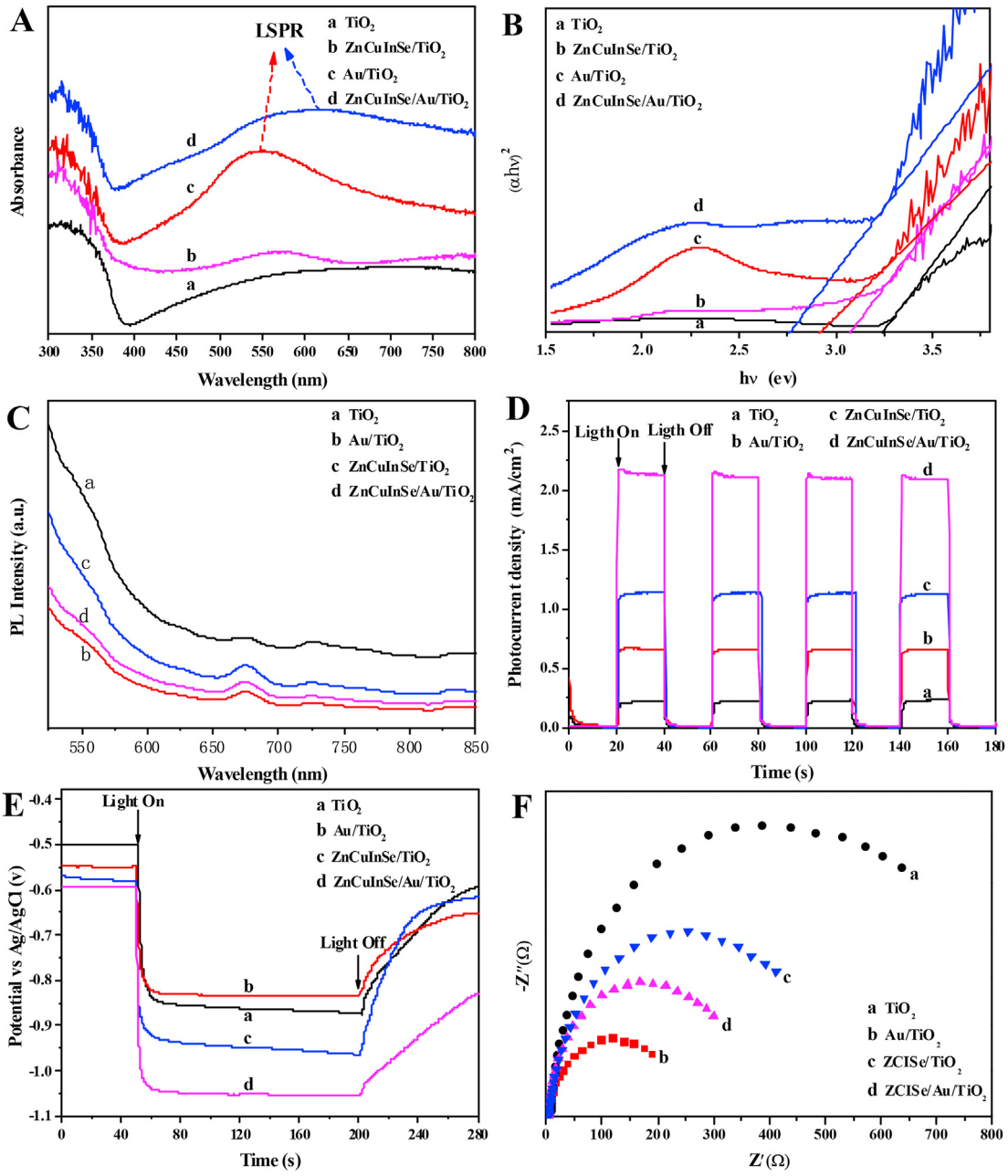

Fig. 2. (A) UV–vis absorption spectra; (B) Optical band-gap; (C) Photoluminescence spectrum; (D) Photocurrent density; (E) The open-circuit potentia response and (F) EIS analysis of different electrodes in sulfide–sulfite electrolyte.

of Au/TiO_2 and $ZnCuInSe/TiO_2$, indicating the synergistic effect of Au NPs and ZnCuInSe QDs. The synergistic effect was caused by enhanced the light absorption of the ZnCuInSe QDs due to increased light scattering of Au NPs [32]. Moreover, Fig. S2D shows the photocurrent density of $ZnCuInSe/Au/TiO_2$ nanowires under light on/off irradiation cycles for 400 s, and Fig. S2E is the photocurrent responses after different storage time. No obvious changes in the responses can be found, indicating a high stability. The open-circuit voltage response was conducted to explore the composite dynamics of the carrier within the electrode, as shown in Fig. 2E. The open-circuit voltage of $ZnCuInSe/Au/TiO_2$ nanowires was more negative than TiO_2 nanowires, suggesting a more accumulation of photogenerated electrons. It is worth noting that the open-circuit voltage of Au/TiO_2 nanowires was lower than that of TiO_2 nanowires, because the interfacial energy states created at $Au–TiO_2$ nanowires contacts could enhance interfacial recombination losses, thus causing decreased voltages. In addition, the open circuit voltage of the electrode begin to decay after the light was turn off, a slow decay rate of the voltage indicates a long electron hole pairs lifetime. The response time was obtained by the reciprocal of the derivative of the decay curve normalized by the thermal voltage [33].

$$\tau n = \frac{-K_B T}{e}\left(\frac{dt}{dVoc}\right) \quad (2)$$

As shown in Fig. S2F, the $ZnCuInSe/Au/TiO_2$ nanowires has the longest response time, which is consistent with the character of

photocurrent density. Moreover, electrochemical impedance spectra (EIS) were recorded to investigate the electrochemical properties of the electrodes, the semicircle diameter from the Nyquist plot of EIS measurement indicates the interfacial charge-transfer resistance of the electrode, as shown in Fig. 2F, the charge transfer resistance decreases after the deposition of Au NPs and ZnCuInSe QDs, most likely because the introduction of Au NPs and ZnCuInSe QDs accelerated electron transfer on the electrode. The increase in resistance of the ZnCuInSe/Au/TiO_2 nanowires than that of the Au/TiO_2 nanowires, this is because the resistance of ZnCuInSe QDs is much higher than that of Au NPs.

3.2. Fabrication of the PEC sensor and optimization of detection conditions

The PEC aptasensor was construced by successive modifications of aptamer and 1% BSA on the ZnCuInSe/Au/TiO_2 electrode. With the successive modifications of kanamycin aptamer and BSA, the photocurrent density decreases (Fig. 3A curves b and c). The presence of aptamer molecules and BSA enhances the steric hindrance of the electrode surface, which blocks the transfers of electrons and electroactive species such as AA on the interface between electrode and electrolyte resulting in decreases in photocurrent density. The stepwise modification process of the aptasensor was also monitored by the EIS method. As shown in Fig. 3B, after successive modification with the kanamycin aptamer and BSA, the resistance increased gradually, owing to the strong steric hindrance and insulation effect of proteins on PBS. The EIS results display that the biosensing platform is constructed successfully according to Scheme 1.

The aptamer concentration, AA concentration, pH of the electrolyte and the binding time of the aptasensor with kanamycin are vital influence factors for the photocurrent density and sensitivity of the sensor. So, the experimental parameters were optimized and the best experimental parameters were obtained based on the photocurrent density. Fig. S3A, B, C and D show the aptamer concentration, AA concentration, pH and binding time-dependent photocurrent density responses, respectively. The optimal experimental parameters are 2.0 μM of aptamer, 0.08 M of AA, pH 7.4, and binding time of 80 min. The decline of photocurrent density at higher AA concentration can be accredit to the decreased absorbance of the electrolyte, which thus decreases the irradiation intensity and formation efficiency of excited electron-hole center [34].

3.3. Quantitative detection of kanamycin and selectivity, reproducibility, stability test of the PEC sensor

Fig. 4A displays the kanamycin concentration-dependent photocurrent density responses. The response is fast and reproducible, and the photocurrent density is basically unchanged after two cycles, indicating that the sensor is stable. Based on a background corrected current ($\Delta I = I_0 - I$, where I_0 and I are the photocurrents before and after incubating with kanamycin, respectively), Fig. 4B shows a logarithmic calibration relationship in the linear range of 0.2 and 250 nM of kanamycin with a regression equation $\Delta I/\mu A = 15.48 \log C + 17.98$, a correlation coefficient of 0.998, and a limit of detection (LOD) of 0.2 nM, the lowest detectable concentration.

Good selectivity, reproducibility and stability are essential to a biosensor. The selectivity was investigated by determining various antibiotics, including chloramphenicol, erythromycin, ciprofloxacin, ofloxacin, doxycycline, and streptomycin. From Fig. 4C, the aptasensor has lower responses to antibiotics other than kanamycin, moreover, a high photocerrent is also observed in the mixture sample including kanamycin and all of the above interferents, the value is slightly smaller than that in the kanamycin sample without interferents, indicating a high selectivity of the aptasensor towards kanamycin.

The inter-assay and intra-assay precision were conducted for the evaluation of the reproducibility. Six identical aptasensors were prepared to detect 200 nM kanamycin. The intra-assay was carried out by testing 200 nM kanamycin for three times with one aptasensor under identical experimental conditions. The relative standard deviation of inter-assay and intra-assay was 5.1% and 4.9%, respectively, suggesting a good reproducibility of the aptasensor. Also, there almost had no changes from the original photocurrent when storing the sensor for 4, 8 and 12 days, respectively, as shown in Fig. 4D, indicating the good long-term stability of the aptasensor.

In Table 1, the performances of the aptasensor were compared with the previously reported methods for the detection of kanamycin based on the linear range and sensitivity. The proposed aptasensor exhibited a comparable or higher sensitivity than reported results.

3.4. Detection of kanamycin in spiked human serum samples

The performance of the sensors in the analysis of actual samples was evaluated by analyzing four human serum samples spiked with various kanamycin concentrations. The results are shown in Table 2.

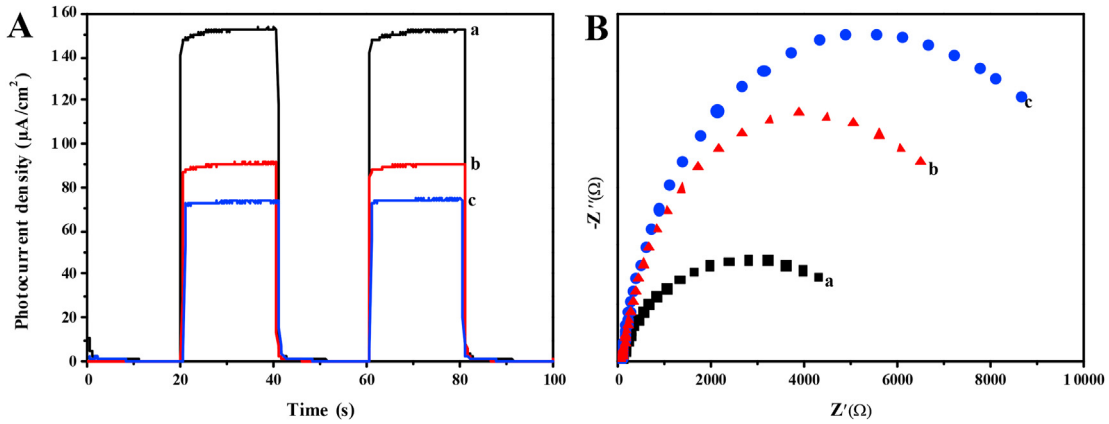

Fig. 3. (A) Photocurrent density amd (B) EIS analysis of (a) ZnCuInSe/Au/TiO_2 nanowires, (b) aptamer/ZnCuInSe/Au/TiO_2 nanowires, and (c) BSA/aptamer/ZnCuInSe/Au/TiO_2 nanowires in PBS (pH 7.4) containing 0.08 M AA.

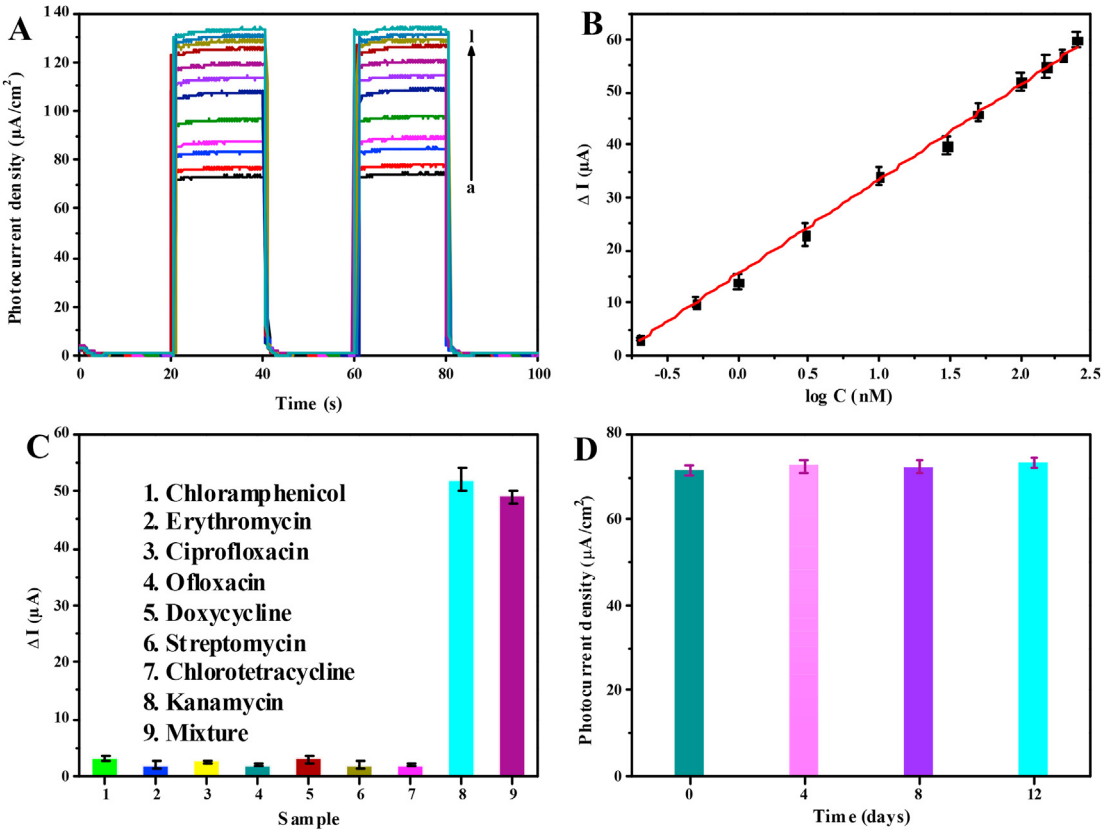

Fig. 4. (A) Photocurrent responses of BSA/aptamer/ZnCuInSe/Au/TiO_2 toward different concentrations of kanamycin: (a) 0, (b) 0.2, (c) 0.5, (d) 1, (e) 3, (f) 10, (g) 30, (h) 50, (i) 100, (j) 150, (k) 200, (l) 250 nM. (B) The calibration curve of the aptasensor for the kanamycin detection. (C) Selectivity of the PEC aptasensor to 200 nM kanamycin and the tabulated antibiotics in PBS (pH 7.4) containing 0.08 M AA, the mixture containing kanamycin, and eight interferents. (D) The photocurrent density of the PEC aptasensor with different storage time.

Table 1
Comparison of different methods for kanamycin detection.

Analytical method	Linear range/nM	Detection limit/nM	References
Colorimetry	1–100	1.49	[35]
Electrochemistry	2.1–128.7	0.1888	[36]
Electrochemistry	10–150	5.8	[37]
Fluorescence	10–1 × 10^3	2.7	[38]
Fluorescence	24.75–137.15	7.5	[39]
PEC	0.2–250	0.2	This work

Table 2
Detection of kanamycin in human serum samples using the sensors.

Sample	Blank (nM)	Added (nM)	Found (nM)	Recovery (%)
1	0	0	0	0
2	2	0.5	2.48	99.2
3	2	10	11.72	97.7
4	2	50	50.3	96.7
5	2	200	196.6	97.3

The recovery rate were 96.0%, 97.2%, 96.6% and 97.3%, respectively, demonstrating a good performance of the aptasensor in the detection of kanamycin in actual samples.

4. Conclusion

A label-free ultrasensitive PEC aptasensor was developed by modification of aptamer on ZnCuInSe/Au/TiO_2 nanowires ternary composite for the detection of kanamycin. The ZnCuInSe QDs formed a cascade band edge structure with TiO_2 nanowires extending the light absorption to visible range and promoting the separation of electrons-hole pairs, while Au NPs act as an electron relay facilitating charge transfer between the ZnCuInSe QDs and TiO_2 nanowires. Additionally, Au NPs on the ZnCuInSe/Au/TiO_2 nanowires significantly improved the PEC performance because of the localized surface plasmon resonance effect. Owing to the high photocurrent density, the proposed aptasensor exhibited a high sensitivity with a LOD down to 0.2 nM and a wide linear range from 0.2 nM to 250 nM. Furthermore, the PEC aptasensor has high stability, selectivity, sensitivity, and acceptable reproducibility. By changing the recognizers, the proposed sensing platform could be easily extended to detect other biomolecules.

CRediT authorship contribution statement

Hongchao Geng: Conceptualization, Methodology, Writing - original draft. **Xiaoxu Chen:** Investigation, Data curation, Writing - review & editing. **Leilei Sun:** Visualization, Formal analysis. **Yan Qiao:** Resources, Visualization. **Jie Song:** Conceptualization. **Sisi Shi:** Resources. **Qingyun Cai:** Funding acquisition, Project administration.

Declaration of competing interest

The authors declare that they have no known competing financial interests or personal relationships that could have appeared to influence the work reported in this paper.

Acknowledgments

We gratefully acknowledge the National Natural Science Foundation of China (Grants No21874038) for financial support.

Appendix A. Supplementary data

Supplementary data to this article can be found online at https://doi.org/10.1016/j.aca.2020.11.017.

References

[1] Y. Chu, A. Deng, W. Wang, J. Zhu, Concatenated catalytic hairpin assembly/hyperbranched hybridization chain reaction based enzyme-free sgnal amplification for the sensitive photoelectrochemical detection of human telomerase RNA, Anal. Chem. 91 (2019) 3619–3627.
[2] J. Li, X. Lin, Z. Zhang, Z Dai W Tu, Red light-driven photoelectrochemical biosensing for ultrasensitive and scatheless assay of tumor cells based on hypotoxic $AgInS_2$ nanoparticles, Biosens. Bioelectron. 126 (2019) 332–338.
[3] W. Zhao, J. Xu, H. Chen, Photoelectrochemical detection of metal ions, Analyst 141 (2016) 4262–4271.
[4] Q. Jiang, H. Wang, X. Wei, Y. Wu, C. Zhu, Efficient $BiVO_4$ photoanode decorated with $Ti_3C_2T_X$ MXene for enhanced photoelectrochemical sensing of Hg(II) ion, Anal. Chim. Acta 1119 (2020) 11–17.
[5] Y. Niu, H. Xie, G. Luo, Y. Zhuang, X. Wu, ZnO-reduced graphene oxide composite based photoelectrochemical aptasensor for sensitive Cd(II) detection with methylene blue as sensitizer, Anal. Chim. Acta 1118 (2020) 1–8.
[6] A. Liu, K. Yin, L. Mi, M. Ma, Y. Liu, S. Liu, A novel photoelectrochemical immunosensor by integration of nanobody and ZnO nanorods for sensitive detection of nucleoside diphosphatase kinase-A, Anal. Chim. Acta 973 (2017) 82–90.
[7] C. Ocaña, S. Lukic, M.D. Valle, Aptamer-antibody sandwich assay for cytochrome c employing an MWCNT platform and electrochemical impedance, Microchim. Ichnoanal. Acta 182 (2015) 2045–2053.
[8] J. Shu, Z. Qiu, J. Zhuang, M. Xu, D. Tang, In situ generation of electron donor to assist signal amplification on porphyrin-sensitized titanium dioxide nanostructures for ultrasensitive photoelectrochemical immunoassay, ACS Appl. Mater. Interfaces 7 (2015) 23812–23818.
[9] Y. Fu, K. Zou, M. Liu, X. Zhang, C. Du, J. Chen, Highly selective and sensitive photoelectrochemical sensing platform for VEGF165 assay based on the switching of photocurrent polarity of CdS QDs by porous Cu_2O-CuO flower, Anal. Chem. 90 (2020) 1189–1196.
[10] X. Li, P. Liu, Y. Tang, L. Yang, L. Li, Z. Qi, D. Li, A photoelectrochemical aptasensor based on a 3D flower-like TiO_2-MoS_2-gold nanoparticle heterostructure for detection of kanamycin, Biosens. Bioelectron. 112 (2018) 193–201.
[11] Y. Luo, X. Tan, D. Young, Q. Chen, Y. Huang, D. Feng, A photoelectrochemical aptasensor for the sensitive detection of streptomycin based on a TiO_2/BiOI/BiOBr heterostructure, Anal. Chim. Acta 1115 (2020) 33–40.
[12] Y. Zhang, M. Li, H. Wang, R. Yuan, S. Wei, Supersensitive photoelectrochemical aptasensor based on Br, N-codoped TiO_2 sensitized by quantum dots, Anal. Chem. 91 (2019) 10864–10869.
[13] H. Geng, P. Du, Z. Zhang, L. Yao, K. Cao, S. Li, P. Sheng, Architecting Bi_2S_3/graphene quantum dots/TiO_2 photoelectrodes for aqueous Cr(VI)/methyl orange removal, Mater. Lett. 214 (2018) 146–149.
[14] R. Wang, M. Zu, S. Yang, S. Zhang, W. Zhou, Z. Mai, S. Zhang, Visible-light-driven photoelectrochemical determination of Cu^{2+} based on CdS sensitized hydrogenated TiO_2 nanorod arrays, Sensor. Actuator. B Chem. 270 (2018) 270–276.
[15] J. Li, S. Cushing, P. Zheng, T. Senty, F. Meng, A.D. Bristow, A. Manivannan, N.Q. Wu, Solar hydrogen generation by a CdS-Au-TiO_2 sandwich nanorod array enhanced with Au nanoparticle as electron relay and plasmonic photosensitizer, J. Am. Chem. Soc. 136 (2014) 8438–8449.
[16] X. Qin, Q. Wang, L. Geng, X. Shu, Y. Wang, A "signal-on" photoelectrochemical aptasensor based on graphene quantum dots-sensitized TiO_2 nanotube arrays for sensitive detection of chloramphenicol, Talanta 197 (2019) 28–35.
[17] R. Moakhar, A. Dolati, M. Ghorbani, Sunlight-driven photoelectrochemical sensor for direct determination of hexavalent chromium based on Au decorated rutile TiO_2 nanorods, Appl. Catal. B Environ. 201 (2017) 411–418.
[18] L. Zhang, Z. Pan, W. Wang, J. Du, Z. Ren, Q. Shen, X. Zhong, Copper deficient Zn-Cu-In-Se quantum dot sensitized solar cells for high efficiency, J. Mater. Chem. 5 (2017) 21442–21451.
[19] X. Zhong, M. Han, Z. Dong, T. White, W. Knoll, Composition-tunable $Zn_xCd_{1-x}Se$ nanocrystals with high luminescence and stability, J. Am. Chem. Soc. 125 (2003) 8589–8594.
[20] R. Zhang, T. Deng, J. Wang, G. Wu, S. Li, Y. Gu, D. Deng, Organic-to-aqueous phase transfer of Zn–Cu–In–Se/ZnS quantum dots with multifunctional multidentate polymer ligands for biomedical optical imaging, New J. Chem. 41 (2017) 5387–5394.
[21] J. Du, Z. Du, J. Hu, Z. Pan, Q. Shen, J. Sun, D. Long, H. Dong, L. Sun, X. Zhong, L. Wan, Zn-Cu-In-Se quantum dot solar cells with a certified power conversion efficiency of 11.6%, J. Am. Chem. Soc. 138 (2016) 4201–4209.
[22] Y. Xu, T. Han, X. Li, L. Sun, Y. Zhang, Colorimetric detection of kanamycin based on analyte-protected silver nanoparticles and aptamer-selective sensing mechanism, Anal. Chim. Acta 891 (2015) 298–303.
[23] N. Zhou, J. Luo, J. Zhang, Y. You, Y. Tian, A label-free electrochemical aptasensor for the detection of kanamycin in milk, Anal. Methods 7 (2015) 1991–1996.
[24] N. Zhou, J. Zhang, Y. Tian, Aptamer-based spectrophotometric detection of kanamycin in milk, Anal. Methods 6 (2014) 1569–1574.
[25] L. Wang, W. Gu, P. Sheng, Z. Zhang, B. Zhang, Q. Cai, A label-free cytochrome c photoelectrochemical aptasensor based on CdS/$CuInS_2$/Au/TiO_2 nanotubes, Sensor. Actuator. B Chem. 281 (2019) 1088–1096.
[26] D. Baker, P. Kamat, Photosensitization of TiO_2 nanostructures with CdS quantum dots, Adv. Funct. Mater. 19 (2009) 805–811.
[27] J. Li, S. Cushing, J. Bright, F. Meng, T. Sentry, P. Zheng, A. Bristow, N. Wu, Ag@Cu_2O Core-shell nanoparticles as visible-light plasmonic photocatalysts, ACS Catal. 3 (2013) 47–51.
[28] A. Hassanien, A. Akl, Influence of composition on optical and dispersion parameters of thermally evaporated non-crystalline $Cd_{50}S_{50-x}Se_x$ thin films, J. Alloys Compd. 648 (2015) 280–290.
[29] C. Liu, X. Dong, Y. Hao, X. Wang, H. Ma, X. Zhang, Efficient photocatalytic dye degradation over Er-doped BiOBr hollow microspheres wrapped with graphene nanosheets: enhanced solar energy harvesting and charge separation, RSC Adv. 7 (2017) 22415–22423.
[30] Y. Chen, X. Bai, A review on quantum dots modified g-C_3N_4-based photocatalysts with improved photocatalytic activity, Catalyst 10 (2020) 142–172.
[31] T. Luttrell, S. Halpegamage, J. Tao, A. Kramer, E. Sutter, M. Batzill, Why is anatase a better photocatalyst than rutile? - model studies on epitaxial TiO_2 films, Sci. Rep. 4 (2014) 4043–4045.
[32] L. Liu, G. Wang, Y. Li, CdSe quantum dot-sensitized Au/TiO_2 hybrid mesoporous films and their enhanced photoelectrochemical performance, Nano Res 4 (2011) 249.
[33] J. Bisquert, A. Zaban, M. Greenshtein, I. Mora-Seró, Determination of rate constants for charge transfer and the distribution of semiconductor and electrolyte electronic energy levels in dye-sensitized solar cells by open-circuit photovoltage decay method, J. Am. Chem. Soc. 126 (2004) 13550–13559.
[34] X. Wang, R. Xu, X. Sun, et al., Using reduced graphene oxide-Ca:CdSe nanocomposite to enhance photoelectrochemical activity of gold nanoparticles functionalized tungsten oxide for highly sensitive prostate specific antigen detection, Biosens. Bioelectron. 96 (2017) 239–245.
[35] T. Sharma, R. Ramanathan, P. Weerathunge, M. Mohammadtaheri, H. Daima, R. Shukla, V. Bansal, Aptamer-mediated 'turn-off/turn-on' nanozyme activity of gold nanoparticles for kanamycin detection, Chem. Commun. 50 (2014) 15856–15859.
[36] A. Sharma, G. Istamboulie, A. Hayat, G. Catanante, S. Bhand, J. Marty, Disposable and portable aptamer functionalized impedimetric sensor for detection of kanamycin residue in milk sample, Sensor. Actuator. B Chem. 245 (2017) 507–515.
[37] X. Sun, F. Li, G. Shen, J. Huang, X. Wang, Aptasensor based on the synergistic contributions of chitosan–gold nanoparticles, graphene–gold nanoparticles and multi-walled carbon nanotubes-cobalt phthalocyanine nanocomposites for kanamycin detection, Analyst 139 (2014) 299–308.
[38] X. Lin, L. Cui, Y. Huang, Y. Lin, Y. Xie, Z. Zhu, B. Yin, X. Chen, C. Yang, Carbon nanoparticle-protected aptamers for highly sensitive and selective detection of biomolecules based on nuclease-assisted target recycling signal amplification, Chem. Commun. 50 (2014) 7646–7648.
[39] S. Dehghani, N. Danesh, M. Ramezani, M. Alibolandi, P. Lavaee, M. Nejabat, A label-free fluorescent aptasensor for detection of kanamycin based on dsDNA-capped mesoporous silica nanoparticles and Rhodamine B, Anal. Chim. Acta 1030 (2018) 142–147.